Monthly Notices of the ROYAL ASTRONOMICAL SOCIETY

MNRAS **538,** 92–100 (2025) https://doi.org/10.1093/mnras/staf296
Advance Access publication 2025 February 18

Theoretical study of Th III energy levels and transitions for applications to kilonova spectra

L. Kitovienė [1]★ G. Gaigalas [1] P. Rynkun [1] N. Domoto,[2] M. Tanaka [2,3] and D. Kato [4,5]

[1]*Institute of Theoretical Physics and Astronomy, Vilnius University, Saulėtekio Ave. 3, LT-10257 Vilnius, Lithuania*
[2]*Astronomical Institute, Tohoku University, Sendai 980-8578, Japan*
[3]*Division for the Establishment of Frontier Sciences, Organization for Advanced Studies, Tohoku University, Sendai 980-8577, Japan*
[4]*National Institute for Fusion Science, 322-6 Oroshi-cho, Toki 509-5292, Japan*
[5]*Interdisciplinary Graduate School of Engineering Sciences, Kyushu University, Kasuga, Fukuoka 816-8580, Japan*

Accepted 2025 February 13. Received 2025 February 13; in original form 2024 December 11

ABSTRACT

The neutron star merger is a promising site of heavy element production. By producing heavy elements, the neutron star merger gives rise to a thermal transient called a kilonova. Studying kilonova spectra enables us to quantify the heavy element production. Among the heaviest elements, doubly ionized Thorium (Th, $Z = 90$) is one of the important candidates for producing detectable absorption features in kilonova spectra. This paper investigates the atomic properties of Th III to provide energy level and transition data. The multiconfiguration Dirac–Hartree–Fock and relativistic configuration interaction methods, which are implemented in the general-purpose relativistic atomic structure package GRASP2018, are used to compute energy levels of the 5f6d, $6d^2$, $7s^2$, $5f^2$, 6d7s, 5f7p and 5f7s configurations and electric dipole transitions between states of these configurations. The accuracy of energy levels is evaluated by comparing it with experimental data and with various theoretical methods. Our calculated energy levels are consistent with the experimental results with a root mean square deviation of 436 cm^{-1}. The accuracy of transition data is investigated using the quantitative and qualitative evaluation method. By performing radiative transfer simulations for kilonova spectra with our transition data, we show that kilonova including Th with a mass fraction of $(3 - 10) \times 10^{-5}$ can produce Th III absorption features around 18 000 Å.

Key words: atomic data – opacity – neutron star mergers.

1 INTRODUCTION

Atomic data of heavy elements are crucially important to understanding spectroscopic features of astronomical objects. In particular, recent observations of a neutron star merger and subsequent electromagnetic signal 'kilonova' (GW170817/AT2017gfo, Abbott et al. 2017) enabled us to study the heavy element production in the Universe directly. For AT2017gfo, extensive time series of optical and near-infrared spectra have been obtained (e.g. Chornock et al. 2017; Pian et al. 2017; Smartt et al. 2017). In these spectra, several heavy elements have been identified/proposed, including Sr (Watson et al. 2019; Domoto et al. 2021; Gillanders et al. 2022), Y (Sneppen & Watson 2023), La (Domoto et al. 2022), and Ce (Domoto et al. 2022, 2023; Tanaka et al. 2023; Gaigalas et al. 2024; Gillanders et al. 2024) as absorption features, and Te (Hotokezaka et al. 2023) as an emission feature.

As a site of heavy element production, one of the most critical questions is how heavy elements are synthesized in neutron star mergers. In particular, the production of actinides ($Z = 89 - 103$) has been of great interest for the nucleosynthesis in neutron star mergers (e.g. Holmbeck et al. 2019; Wanajo et al. 2022) as well as its connection to the abundances found in metal-poor stars (see e.g. Cowan et al. 2021 for a review). To understand the impact of actinides on kilonova, several works have been performed (Fontes et al. 2020, 2023; Pognan et al. 2024). However, due to a lack of accuracy, these works only focus on the statistical properties of actinides.

Recently, Domoto et al. (2024) compiled spectroscopically accurate atomic data for Th III and suggested that Th III lines can show absorption features in kilonova spectra at near-infrared wavelengths. However, in their work, transition probabilities (and oscillator strengths) of Th III lines have been estimated by using the emission line ratios measured in the thorium–argon hollow cathode lamp spectrum Engleman (2003) together with calculations by Biémont, Quinet & Ryabchikova (2002a, see below). Thus, the accuracy of the transition probabilities is hard to estimate. To assess the detectability of Th III lines in the kilonova spectra, it is essential to provide accurate and systematic transition data, particularly in the infrared wavelength ranges.

Several experimental and theoretical works on Th III, are described below. In the first papers, the authors used the Zeeman patterns to analyse the Th III spectrum. de Bruin & Klinkenberg (1940) investigated the patterns of the lines in the wavelengths range 2099.42–4555.64 Å and reported 50 identified energy levels. de Bruin, Klinkenberg & Schuurmans (1941) have observed about 200 lines in the wavelength range 2000–9000 Å and identified 77 energy levels of the 5f, {7s, 7p, 6d}, $5f^2$, 6d{7s, 7p}, 7p7s, $6d^2$ configurations.

★ E-mail: laima.radziute@tfai.vu.lt

The number of identified lines was increased significantly using sliding spark spectrum by Wyart & Kaufman (1981). The authors measured the sliding spark spectrum in the 500–1500 Å range. In this study, 488 lines were classified as transitions between 98 new levels and 77 previously known levels. The interpretation of the $5f^2$ and 5f6d configurations has been completed and the main properties of 5f{6f, 8p}, and 6d{7d, 6f} were described. All of these configurations have been interpreted using the Slater–Condon theory.

Biémont et al. (2002b) have measured lifetimes of six levels, with the time-resolved laser-induced fluorescence (LIF) technique. The properties of the transitions depopulating these levels were computed using pseudo-relativistic Hartree–Fock (HFR) method (Cowan 1981) and normalized with the experimental lifetimes. The first set of transition probabilities have been deduced for Th III by these authors.

Several theory-based studies of this ion have been carried out in recent decades. Berengut et al. (2009) have computed eleven energy levels using a combination of second-order many-body perturbation theory and configuration interaction, which considers dominating relativistic and correlation effects (CI+MBPT). Later, Safronova, Safronova & Clark (2014) have determined energy levels, transition properties, and lifetimes with configuration-interaction plus all-order (CI+all) method. This method combines CI and coupled-cluster approaches. Roy et al. (2012) have conducted a series of relativistic spin-free calculations at state-average complete active space self-consistent field (SA-CASSSCF) for energy levels and transition properties. The dynamic electron correlation effects have been studied through second-order perturbation theory that has been performed at multistate second-order multiconfigurational perturbation theory (MS-CASPT2) level. In both cases, the spin-orbit treatments at SA-CASSCF and MS-CASPT2 levels have been performed using an effective Fock-type one-electron spin-orbit operator.

The most recent experiment was done by Redman, Nave & Sansonetti (2014). They have made precise and extensive observations of a thorium–argon hollow cathode lamp emission spectrum in 3500–11750 Å region, using a high-resolution Fourier transform spectrometer. This investigation led to new energy levels of doubly ionized thorium, and these levels are referred to in the National Institute of Standards and Technology (NIST) (Kramida et al. 2021).

As described above, despite its importance in kilonova spectra, the number of papers addressing the properties of Th III is still limited. Also, as seen from the energy level analysis below, the energy information for the configurations chosen by the authors is incomplete, as is the transition information between these levels. It is also worth noting that the discrepancy between the calculated energy level and the experimental values is huge in some authors' theoretical works. Therefore, we have decided to research using the GRASP2018 programme package.

We have computed 63 energy levels of the 5f{7s, 6d, 7p}, $6d^2$, $5f^2$, $7s^2$, and 6d7s configurations, using multiconfiguration Dirac–Hartree–Fock (MCDHF) and relativistic configuration interaction (RCI) methods. Transitions of E1 were computed between these levels. The GRASP2018 package was used for the investigation (Jönsson et al. 2023).

2 COMPUTATIONAL PROCEDURE

2.1 Methods

The calculations were performed using the GRASP2018 package (Jönsson et al. 2023), which is based on the MCDHF and RCI methods. The first method was used to generate numerical representations of atomic state functions (ASFs). The angular integrations needed for the construction of the functional energy are based on second quantization in the coupled tensorial form (Gaigalas, Rudzikas & Fischer 1997; Gaigalas, Fritzsche & Grant 2001). The Breit interaction, as well as quantum electrodynamic corrections, are included using the second method. ASFs are transformed from the $jj-$ to the $LS-$coupling with a unique representation (Gaigalas et al. 2017). The method described by (Gaigalas 2020) was used to transform the other couplings. The quantitative and qualitative evaluation method (QQE) (Gaigalas et al. 2022; Rynkun et al. 2022; Radžiūtė & Gaigalas 2023; Kitovienė et al. 2024) was used to estimate the uncertainty of the calculated line strengths. More details about these methods can be found in Fischer et al. (2016) and Grant (2007).

2.2 Correlation inclusions scheme

For the calculations, the core was assumed to be the $[Xe]4f^{14}5d^{10}6s^26p^6$ shells. The radial wave functions of the core orbitals were calculated using the Single Reference configuration method and the $[Xe]4f^{14}5d^{10}6s^26p^65f7s$ configuration was selected for it like that was done in the works of Radžiūtė et al. (2020) and Radžiūtė et al. (2021). The valence orbitals {7s, 7p, 6d, 5f} were computed in the Multi-reference configuration (MR) approach, the 5f{7s, 6d, 7p}, $6d^2$, $5f^2$, $7s^2$, and 6d7s configurations were selected for the MR set. The sets of virtual orbitals were generated with single and double electron excitations from the configurations in the MR set. Only valence–valence electron correlations were included in this step. Radial functions of virtual orbitals were computed using the multiconfiguration Dirac–Hartree–Fock method. The calculations were carried out step by step (or layer by layer, keeping the previous layer frozen). The four layers of virtual orbitals (up to 11s, 11p, 10d, 9f, 8g) were computed until convergence of the energy levels was achieved.

For further RCI calculations, the configurations were divided into three groups. The first group consists of the 5f{6d, 7s} configurations, the second group consists of $6d^2$, $7s^2$, and 6d7s, and the third group includes only the $5f^2$ and 5f7p configurations. Core-valence electron correlations of 5d6s6p shells were included for all three groups.

The MR set for computation of the energy levels of the 5f{6d, 7s} configurations (the first group) was extended by 7s7p and 6d7p configurations. Core–core (CC) of 6p were included in RCI computations.

The energy levels of the $6d^2$, $7s^2$, and 6d7s configurations set (the second group) were computed using the MR set: $6d^2$, $7s^2$, $5f^26d7s$, and 5f7p and CC correlations of the shells 6s6p were added.

To compute the energy levels of the $5f^2$ and 5f7p configurations set (the third group) of $6d^2$, $7s^2$, $5f^26d7s$, and 5f7p configurations were used as the MR and CC correlations of the 6p shells were included.

The final results (RCI) are computed in the basis of 6227 777 configuration state functions (CSF) for even and 3426 892 for odd parity. The final energy levels are given in Tables 1 and 2 for odd and even configurations, respectively.

3 RESULTS

3.1 Comparison of energy levels

The accuracy of our computed energy levels (RCI) is evaluated by comparing with experimental data by Redman et al. (2014) and theoretical data. Safronova et al. (2014) studied energy levels of 5f{7s, 8s, 6d, 7d}, and 6d7p odd-parity and of $6d^2$, $5f^2$, $7s^2$,

Table 1. Comparison of the lowest energy levels (in cm^{-1}) of ours (RCI), Safronova et al. (2014) (CI+all), Berengut et al. (2009) (CI+MBPT), Roy et al. (2012) (SA-CASSCF and MS-CASPT2) with the experimental (Redman et al. 2014) (Ex.) values for odd configurations.

No.	Label	J	P	Ex.	CI+all		CI+MBPT		SA-CASSCF		MS-CASPT2		RCI	
				E	E	ΔE	E	ΔE	E	ΔE	E	ΔE	E	ΔE
31	5f6d ^{3}P	0	–	11 233	11 766	−533							11 567	−334
21	5f6d ^{3}D	1	–	7921	8260	−339							8155	−234
30	5f6d ^{3}P	1	–	11 123	11 564	−441							11 466	−343
43	5f6d ^{1}P	1	–	20 711	22 733	−2022							21 789	−1078
3	5f6d ^{3}F	2	–	511	189	322			6933	−6422	1074	−563	469	42
6	5f7s ^{3}F	2	–	3182	2958	224			10 671	−7489	5048	−1866	3256	−74
15	5f6d ^{1}D	2	–	6288	5797	491			16 333	−10045	8162	−1874	6243	45
24	5f6d ^{3}D	2	–	10 181	10 458	−277							10 250	−69
33	5f6d ^{3}P	2	–	13 208	13 513	−305							13 431	−223
4	5f7s ^{3}F	3	–	2527	2436	91			12 099	−9572	6879	−4352	2548	−21
9	5f6d ^{3}F	3	–	4827	4853	−26			9316	−4489	4044	783	4810	17
11	5f6d ^{3}G	3	–	5061	5085	−24			7629	−2568	5815	−724	5002	59
18	5f7s ^{1}F	3	–	7501	7609	−108			14 709	−7208	9515	−2014	7630	−129
28	5f6d ^{3}D	3	–	10 741	11 236	−495							10 858	−117
35	5f6d ^{1}F	3	–	15 453	16 506	−1053							15 674	−221
1	5f6d ^{3}H	4	–	0	0	0	0	0	5196	−5196	1713	−1713	0	0
5	5f6d ^{1}G	4	–	3188	3207	−19			8975	−5787	4938	−1750	3040	148
14	5f7s ^{3}F	4	–	6311	6237	74			16 012	−9701	10806	−4495	6199	112
19	5f6d ^{3}G	4	–	8142	8197	−55							8024	118
23	5f6d ^{3}F	4	–	8981	9063	−82			13 033	−4063	7942	1039	8867	114
8	5f6d ^{3}H	5	–	4490	4802	−312			9945	−5455	7176	−2686	4460	30
29	5f6d ^{3}G	5	–	11 277	11 456	−179							11 189	88
39	5f6d ^{1}H	5	–	19 010	20 144	−1135							19 719	−709
22	5f6d ^{3}H	6	–	8437	8810	−373			14 321	−5884	11552	−3115	8272	165

5f{7p, 6f}, and 6d7s even-parity configurations using CI+all approach, while Berengut et al. (2009) have presented only eleven energy levels of $6d^2$, 6d7s, $5f^2$, and 5f7p configurations, using CI+MBPT approach. Roy et al. (2012) have calculated a part of energy levels of 5f{6d, 7s} odd-parity and of $6d^2$, $7s^2$, and 6d7s even-parity using SA-CASSCF and MS-CASPT2 methods. Our calculated energy levels and the differences from the experimental values are given in Tables 1 and 2. Theoretical values calculated by other authors and differences from experimental data are also given in the same tables.

The differences from the experiment are more significant than 1000 cm^{-1} for eight levels of the CI+all method, and for four energy levels for the CI+MBPT method. Meanwhile, almost all levels of the MS-CASPT2 method differ from the experiment by more than a thousand cm^{-1}. The differences are even worse for the levels from the SA-CASSCF method. It should also be noted that the ground state was $6d^2\ ^3F_2$ in both calculations by Roy et al. (2012), and this contradicts the most recent data from Redman et al. (2014). In our study, only five energies differ from the experimental data of Redman et al. (2014) of more than 1000 cm^{-1}. The ground state is also consistent with the experimental findings.

A summary of RMS from the experimental data is given for each configuration, and all levels are compared in Table 3 for all authors. The superscript [1] in Table 3 indicates that the RMS is calculated excluding one energy level, which is more distant from experimental values than the others in that configuration. The energy value of our level $6d^2\ ^1S_0$ is 22 547 cm^{-1} and this value is larger than the Redman et al. (2014) value by 3554 cm^{-1} and also for level $5f^2\ ^1S_0$ our calculated energy of 55 047 is 3885 cm^{-1} higher. RMS calculated with all levels of configuration are given in parentheses.

The RMS deviation of all compared levels is given in the last line ('all') of Table 3. The RMS deviation of all our levels from experimental data is $436^2(796)$ while the deviation of levels from CI+all and CI+MBPT method are larger (891 and 1089). The most significant deviation from experiments is visible for the MS-CASPT2 method (1871) results. The superscript [2] in the table indicates that the RMS is calculated excluding two energy levels mentioned in the above paragraph.

The labels of atomic state functions and composition in $LS-$, $JJ-$couplings of our computations and Blaise & Wyart (1992) and Safronova et al. (2014) are given in Tables 4 and 5. It is important to note that, in a general sense, a jj-coupling is not identical to a JJ-coupling, and that the notation of the terms is also different (Martin & Wiese 1996; Gaigalas 2020). However, in the present case (5f7p–two orbitals with one electron each) the angular momenta are the same in both couplings, therefore the jj-coupling corresponds to the JJ-coupling (Gaigalas 2020). This allows us to use Blaise & Wyart (1992) JJ-coupling identification instead of jj-coupling to analyse the purity of ASF in relativistic scheme calculation.

Labels of the atomic state function (configuration and term) for odd configurations are identical to those presented in Blaise & Wyart (1992) work, even in instances where the CSF mixing is more pronounced (see Table 4). The ASFs of even parity are observed to be more mixed than those of odd parity. Contributions of configuration state functions are marked in bold for the states in which the labels are not assigned with the most significant contribution to the composition. Only the first components of the composition in the $LS-$coupling for ASFs of the 5f7p configuration are provided by Blaise & Wyart (1992), who also based their findings on these terms. However, it should be noted that the identification of ASFs given by Blaise & Wyart (1992) is not unique. In the meantime, we have transformed the ASFs from $jj-$ to the $LS-$coupling with a unique representation, as proposed by Gaigalas et al. (2017). The ASFs for this configuration are purer in the $JJ-$coupling, as demonstrated by Blaise & Wyart (1992). Our computations indicate that the atomic state functions are also less mixed in the $JJ-$coupling than in

Table 2. Comparison of the lowest energy levels (in cm^{-1}) of ours (RCI), Safronova et al. (2014) (CI+all), Berengut et al. (2009) (CI+MBPT), Roy et al. (2012) (SA-CASSCF and MS-CASPT2) with the experimental (Redman et al. 2014) (Ex.) values for even configurations.

No.	Label	J	P	Ex.	CI+all		CI+MBPT		SA-CASSCF		MS-CASPT2		RCI	
				E	E	ΔE	E	ΔE	E	ΔE	E	ΔE	E	ΔE
12	$6d^2\ ^3P$	0	+	5090	6151	−1061							5641	−551
32	$7s^2\ ^1S$	0	+	11 961	12 428	−467			15 309	−3348	12459	−498	12 909	−948
44	$6d^2\ ^1S$	0	+	18 993	22 008	−3015							22 547	−3554
48	$5f^2\ ^3P$	0	+	29 300	29 579	−279							30 429	−1129
63	$5f^2\ ^1S$	0	+	51 162	55 356	−4194							55 047	−3885
13	$6d7s\ ^3D$	1	+	5524	6137	−613			6947	−1423	6520	−996	5998	−474
20	$6d^2\ ^3P$	1	+	7876	8905	−1029			9771	−1895	8272	−396	8088	−212
49	$5f^2\ ^3P$	1	+	30 403	30 636	−233							31 111	−708
58	$5f7p\ ^3D$	1	+	44 603	44 946	−343							44 848	−245
2	$6d^2\ ^3F$	2	+	63	895	−832			0	63	0	63	266	−203
10	$6d^2\ ^1D$	2	+	4676	5426	−750			5451	−775	5003	−327	4926	−250
17	$6d7s\ ^3D$	2	+	7176	7943	−767			8617	−1441	8011	−835	7576	−400
27	$6d^2\ ^3P$	2	+	10 440	11 417	−977			12 356	−1916	11087	−647	10 608	−168
36	$6d7s\ ^1D$	2	+	16 038	16 438	−400			19 163	−3125	17628	−1590	16 265	−227
38	$5f^2\ ^3F$	2	+	18 864	18 616	248							18 869	−5
46	$5f^2\ ^1D$	2	+	28 233	28 971	−738							29 121	−888
50	$5f^2\ ^3P$	2	+	32 867	33 488	−621							33 345	−478
52	$5f7p\ ^3F$	2	+	34 996									35 475	−479
57	$5f7p\ ^3D$	2	+	43 759									44 021	−262
62	$5f7p\ ^1D$	2	+	49 806									50 225	−419
7	$6d^2\ ^3F$	3	+	4056	4938	−882	4023	33	4278	−222	4478	−422	4162	−106
25	$6d7s\ ^3D$	3	+	9954	10 641	−687	9204	750	11 465	−1511	11038	−1084	10 371	−417
41	$5f^2\ ^3F$	3	+	20 840	20 378	462	19068	1772					20 357	483
51	$5f7p\ ^3G$	3	+	33 562	33 715	−153							33 944	−382
53	$5f7p\ ^3F$	3	+	38 432	38 736	−304							38 784	−352
55	$5f7p\ ^1F$	3	+	42 313	42 544	−231							42 459	−146
60	$5f7p\ ^3D$	3	+	47 471	47 876	−405							47 647	−176
16	$6d^2\ ^3F$	4	+	6538	7264	−726	6795	−257	7385	−847	7174	−636	6629	−91
26	$6d^2\ ^1G$	4	+	10 543	10 822	−279	11051	−508	13 567	−3024	11742	−1199	10 439	104
34	$5f^2\ ^3H$	4	+	15 149	14 514	635	13358	1791					14 636	513
42	$5f^2\ ^3F$	4	+	21 784	21 782	2	20366	1418					21 504	280
45	$5f^2\ ^1G$	4	+	25 972	27 045	−1073	25269	703					25 815	157
54	$5f7p\ ^3F$	4	+	38 581	38 980	−399							39 062	−481
56	$5f7p\ ^3G$	4	+	43 702	44 034	−332							44 001	−299
59	$5f7p\ ^1G$	4	+	47 261	47 745	−484							47 581	−320
37	$5f^2\ ^3H$	5	+	17 887	17 131	756	16068	1819					17 202	685
61	$5f7p\ ^3G$	5	+	47 422	47 781	−359							47 956	−534
40	$5f^2\ ^3H$	6	+	20 771	20 123	648							19 972	799
47	$5f^2\ ^1I$	6	+	28 350	28 635	−285							29 422	−1072

Table 3. RMS (in cm^{-1}) of our computed energy levels, of CI+all method (Safronova et al. 2014), of CI+MBPT method (Berengut et al. 2009), and of SA-CASSCF and MS-CASPT2 methods (Roy et al. 2012) from the experiment (Redman et al. 2014), according configurations.

Conf.	CI+all	CI+MBPT	SA-CASSCF	MS-CASPT2	RCI
5f6d	637	–	6160	1885	337
5f7s	137	–	8570	3416	94
$6d^2$	1331	329	1740	636	253^1(1208)
6d7s	580	750	2010	1162	391
$7s^2$	467	–	3348	498	948
$5f^2$	1288	1560	–	–	686^1(1263)
5f7p	347	86	–	–	361
all	891	1089	5113	1871	436^2(796)

the $LS-$coupling. However, they remain more mixed than in the Blaise & Wyart (1992) study (see Table 5). The ASF labels are provided in the $LS-$coupling from the CI+all method without the composition. Sometimes, the terms in the $LS-$coupling from the CI+all method differ from our results and those presented in Blaise & Wyart (1992).

4 EVALUATION OF THE LINE STRENGTHS

In this work, we have calculated 455 E1-type transitions between the energy levels of the configurations mentioned above. QQE method (Gaigalas et al. 2022; Rynkun et al. 2022; Kitovienė et al. 2024) was used to evaluate the uncertainty of the calculated line strengths. Using the QQE method, all these transitions were distributed according to the accuracy classes in Fig. 1. As can be seen, a majority of the transitions are in the E class. According to the QQE method, 46 per cent fall into the D and better accuracy class.

Furthermore, our calculated transition data have been compared with the results of studies carried out by other authors. Initially, a comparison was made between the transition probabilities that originated from two states, specifically $5f^2\ ^3P_2$ and $5f7p\ ^3F_4$. The HFR method was employed by Biémont et al. (2002b) to compute the transition probabilities for these states and then normalized according

Table 4. ASFs labels for present (RCI) work and composition (in percentages) in LS-coupling from Blaise & Wyart (1992) and Safronova et al. (2014) (CI+all) studies.

No.	RCI labels	Compositions		CI+all labels
		RCI	Blaise & Wyart (1992)	
31	$5f6d\ ^3P^\circ_0$	92	99 + 1 $6d7p\ ^3P^\circ$	...
21	$5f6d\ ^3D^\circ_1$	81 + 6 $5f6d\ ^1P^\circ$ + 5 $5f6d\ ^3P^\circ$	83 + 8 $5f6d\ ^1P^\circ$	$^3D^\circ_1$
30	$5f6d\ ^3P^\circ_1$	80 + 8 $5f6d\ ^3D^\circ$ + 4 $5f6d\ ^1P^\circ$	83 + 11 $5f6d\ ^3D^\circ$	$^3P^\circ_1$
43	$5f6d\ ^1P^\circ_1$	81 + 6 $5f6d\ ^3P^\circ$ + 3 $5f6d\ ^3D^\circ$	86 + 7 $5f6d\ ^3P^\circ$	$^1P^\circ_1$
3	$5f6d\ ^3F^\circ_2$	61 + 20 $5f6d\ ^1D^\circ$ + 11 $5f7s\ ^3F^\circ$	60 + 23 $5f6d\ ^1D^\circ$	$^3F^\circ_2$
6	$5f7s\ ^3F^\circ_2$	76 + 13 $5f6d\ ^1D^\circ$ + 2 $5f6d\ ^3F^\circ$	80 + 14 $5f6d\ ^1D^\circ$	$^3F^\circ_2$
15	$5f6d\ ^1D^\circ_2$	49 + 29 $5f6d\ ^3F^\circ$ + 6 $5f7s\ ^3F^\circ$	49 + 35 $5f6d\ ^3F^\circ$	$^1D^\circ_2$
24	$5f6d\ ^3D^\circ_2$	83 + 6 $5f6d\ ^3P^\circ$ + 2 $5f6d\ ^1D^\circ$	88 + 8 $5f6d\ ^3P^\circ$	$^3D^\circ_2$
33	$5f6d\ ^3P^\circ_2$	79 + 8 $5f6d\ ^1D^\circ$ + 4 $5f6d\ ^3D^\circ$	84 + 9 $5f6d\ ^1P^\circ$	$^3P^\circ_2$
4	$5f7s\ ^3F^\circ_3$	40 + 32 $5f6d\ ^3F^\circ$ + 16 $5f7s\ ^1F^\circ$	47 + 24 $5f6d\ ^3F^\circ$	$^3F^\circ_3$
9	$5f6d\ ^3F^\circ_3$	34 + 25 $5f6d\ ^3G^\circ$ + 18 $5f7s\ ^3F^\circ$	40 + 31 $5f6d\ ^3G^\circ$	$^1F^\circ_3$
11	$5f6d\ ^3G^\circ_3$	54 + 22 $5f6d\ ^3F^\circ$ + 9 $5f7s\ ^1F^\circ$	52 + 28 $5f6d\ ^3F^\circ$	$^3G^\circ_3$
18	$5f7s\ ^1F^\circ_3$	43 + 35 $5f7s\ ^3F^\circ$ + 6 $5f6d\ ^3G^\circ$	43 + 39 $5f7s\ ^3F^\circ$	$^1F^\circ_3$
28	$5f6d\ ^3D^\circ_3$	68 + 16 $5f6d\ ^1F^\circ$ + 4 $5f7s\ ^1F^\circ$	72 + 19 $5f6d\ ^1F^\circ$	$^3D^\circ_3$
35	$5f6d\ ^1F^\circ_3$	61 + 23 $5f6d\ ^3D^\circ$ + 5 $5f7s\ ^1F^\circ$	67 + 25 $5f6d\ ^3D^\circ$	$^3F^\circ_3$
1	$5f6d\ ^3H^\circ_4$	56 + 34 $5f6d\ ^1G^\circ$ + 3 $5f6d\ ^3F^\circ$	64 + 32 $5f6d\ ^1G^\circ$	$^3H^\circ_4$
5	$5f6d\ ^1G^\circ_4$	42 + 36 $5f6d\ ^3H^\circ$ + 14 $5f6d\ ^3F^\circ$	49 + 34 $5f6d\ ^3H^\circ$	$^1G^\circ_4$
14	$5f7s\ ^3F^\circ_4$	44 + 34 $5f6d\ ^3F^\circ$ + 11 $5f6d\ ^1G^\circ$	60 + 26 $5f6d\ ^3F^\circ$	$^3F^\circ_4$
19	$5f6d\ ^3G^\circ_4$	72 + 15 $5f7s\ ^3F^\circ$ + 5 $5f6d\ ^3F^\circ$	75 + 14 $5f7s\ ^3F^\circ$	$^3G^\circ_4$
23	$5f6d\ ^3F^\circ_4$	37 + 32 $5f7s\ ^3F^\circ$ + 18 $5f6d\ ^3G^\circ$	47 + 23 $5f7s\ ^3F^\circ$	$^3F^\circ_4$
8	$5f6d\ ^3H^\circ_5$	93	99 + 1 $5f6d\ ^3G^\circ$	$^3H^\circ_5$
29	$5f6d\ ^3G^\circ_5$	90 + 3 $5f6d\ ^1H^\circ$	96	$^3G^\circ_5$
39	$5f6d\ ^1H^\circ_5$	89 + 3 $5f6d\ ^3G^\circ$	96 + 3 $5f6d\ ^3G^\circ$	$^1H^\circ_5$
22	$5f6d\ ^3H^\circ_6$	93	100	$^3H^\circ_6$
12	$6d^2\ ^3P_0$	66 + 12 $6d^2\ ^1S$ + 8 $5f^2\ ^3P$	65 + 16 $6d^2\ ^1S$	...
32	$7s^2\ ^1S_0$	49 + 26 $6d^2\ ^1S$ + 11 $6d^2\ ^3P$	59 + 20 $6d^2\ ^1S$	...
44	$6d^2\ ^1S_0$	**29** + 36 $7s^2\ ^1S$ + 21 $5f^2\ ^1S$	40 + 35 $7s^2\ ^1S$	...
48	$5f^2\ ^3P_0$	78 + 10 $6d^2\ ^3P$	82 + 14 $6d^2\ ^3P$	...
63	$5f^2\ ^1S_0$	59 + 24 $6d^2\ ^1S$ + 2 $7s^2\ ^1S$	75 + 21 $6d^2\ ^1S$	...
13	$6d7s\ ^3D_1$	90	97 + 2 $5f7p\ ^3D$	$^3D_1$
20	$6d^2\ ^3P_1$	80 + 11 $5f^2\ ^3P$	84 + 15 $5f^2\ ^3P$	$^3P_1$
49	$5f^2\ ^3P_1$	79 + 11 $6d^2\ ^3P$	84 + 15 $5f^2\ ^3P$	$^3P_1$
58	$5f7p\ ^3D_1$	92	97	$^3D_1$
2	$6d^2\ ^3F_2$	65 + 17 $6d^2\ ^1D$ + 4 $5f^2\ ^3F$	65 + 21 $6d^2\ ^1D$	$^3F_2$
10	$6d^2\ ^1D_2$	29 + 18 $6d7s\ ^1D$ + 17 $6d^2\ ^3F$	32 + 22 $6d^2\ ^3F$	$^1D_2$
17	$6d7s\ ^3D_2$	64 + 11 $6d^2\ ^3P$ + 9 $6d^2\ ^1D$	75 + 7 $6d^2\ ^3P$	$^3D_2$
27	$6d^2\ ^3P_2$	58 + 9 $5f^2\ ^3P$ + 9 $6d7s\ ^1D$	64 + 13 $5f^2\ ^3P$	$^3P_2$
36	$6d7s\ ^1D_2$	35 + 20 $5f^2\ ^1D$ + 16 $5f^2\ ^3F$	51 + 19 $5f^2\ ^1D$	$^1D_2$
38	$5f^2\ ^3F_2$	66 + 14 $6d7s\ ^1D$ + 5 $6d^2\ ^1D$	82 + 7 $6d7s\ ^1D$	$^3F_2$
46	$5f^2\ ^1D_2$	44 + 23 $5f^2\ ^3P$ + 11 $6d^2\ ^1D$	50 + 23 $5f^2\ ^3P$	$^3D_2$
50	$5f^2\ ^3P_2$	55 + 19 $5f^2\ ^1D$ + 9 $6d^2\ ^3P$	59 + 21 $5f^2\ ^1D$	$^3P_2$
52	$5f7p\ ^3F_2$	61 + 15 $5f7p\ ^1D$ + 13 $5f7p\ ^3D$	63	–
57	$5f7p\ ^3D_2$	51 + 28 $5f7p\ ^3F$ + 13 $5f7p\ ^1D$	51	–
62	$5f7p\ ^1D_2$	59 + 28 $5f7p\ ^3D$ + 3 $5f7p\ ^3F$	61	–
7	$6d^2\ ^3F_3$	85 + 6 $5f^2\ ^3F$	91 + 8 $5f^2\ ^3F$	$^3F_3$
25	$6d7s\ ^3D_3$	89	96 + 3 $5f7p\ ^3D$	$^3D_3$
41	$5f^2\ ^3F_3$	85 + 6 $6d^2\ ^3F$	91 + 8 $6d^2\ ^3F$	$^3F_3$
51	$5f7p\ ^3G_3$	62 + 23 $5f7p\ ^1F$ + 7 $5f7p\ ^3F$	68 $5f7p\ ^3G$	$^3G_3$
53	$5f7p\ ^3F_3$	41 + 32 $5f7p\ ^3D$ + 18 $5f7p\ ^1F$	42 $5f7p\ ^3F$	$^3F_3$
55	$5f7p\ ^1F_3$	**28** + 34 $5f7p\ ^3F$ + 29 $5f7p\ ^3G$	37 $5f7p\ ^3F$	$^1F_3$
60	$5f7p\ ^3D_3$	55 + 25 $5f7p\ ^1F$ + 11 $5f7p\ ^3F$	55 $5f7p\ ^3D$	$^3F_3$
16	$6d^2\ ^3F_4$	62 + 17 $6d^2\ ^1G$ + 6 $5f^2\ ^3F$	69 + 17 $6d^2\ ^1G$	$^3F_4$

Table 4 – *continued*

No.	RCI labels	Compositions		CI+all labels
		RCI	Blaise & Wyart (1992)	
26	$6d^2\ ^1G_4$	43 + 22 $6d^2\ ^3F$ + 20 $5f^2\ ^1G$	59 + 20 $6d^2\ ^3F$	$^3G_4$
34	$5f^2\ ^3H_4$	84 + 6 $6d^2\ ^1G$	93 + 4 $6d^2\ ^1G$	$^3H_4$
42	$5f^2\ ^3F_4$	68 + 12 $5f^2\ ^1G$ + 6 $6d^2\ ^1G$	63 + 22 $5f^2\ ^1G$	$^3F_4$
45	$5f^2\ ^1G_4$	54 + 18 $6d^2\ ^1G$ + 16 $5f^2\ ^3F$	57 + 26 $5f^2\ ^3F$	$^1G_4$
54	$5f7p\ ^3F_4$	**31** + 44 $5f7p\ ^3G$ + 17 $5f7p\ ^1G$	46 $5f7p\ ^3G$	$^3G_4$
56	$5f7p\ ^3G_4$	47 + 27 $5f7p\ ^1G$ + 18 $5f7p\ ^3F$	51 $5f7p\ ^3G$	$^3G_4$
59	$5f7p\ ^1G_4$	47 + 43 $5f7p\ ^3F$	51 $5f7p\ ^3F$	$^3F_4$
37	$5f^2\ ^3H_5$	92	100	$^3H_5$
61	$5f7p\ ^3G_5$	93	100	$^3G_5$
40	$5f^2\ ^3H_6$	91	97 + 2 $5f^2\ ^1I$	$^3H_6$
47	$5f^2\ ^1I_6$	90	97 + 2 $5f^2\ ^3H$	$^1I_6$

Table 5. Atomic state function labels in $LS-$coupling and in $JJ-$coupling and the compositions in percentages from present computation (RCI) and given by Blaise & Wyart (1992) (Ref.).

No.	RCI label LS	RCI label JJ	JJ Composition in per cent	
			RCI	Ref.
58	$5f\,7p\ ^3D_1$	$5f\,7p\ (5/2,3/2)_1$	93	100
52	$5f\,7p\ ^3F_2$	$5f\,7p\ (5/2,1/2)_2$	83	96
57	$5f\,7p\ ^3D_2$	$5f\,7p\ (5/2,3/2)_2$	88	96
62	$5f\,7p\ ^1D_2$	$5f\,7p\ (7/2,3/2)_2$	89	99
51	$5f\,7p\ ^3G_3$	$5f\,7p\ (5/2,1/2)_3$	92	99
53	$5f\,7p\ ^3F_3$	$5f\,7p\ (7/2,1/2)_3$	88	96
55	$5f\,7p\ ^1F_3$	$5f\,7p\ (5/2,3/2)_3$	91	98
60	$5f\,7p\ ^3D_3$	$5f\,7p\ (7/2,3/2)_3$	88	96
54	$5f\,7p\ ^3F_4$	$5f\,7p\ (7/2,1/2)_4$	89	96
56	$5f\,7p\ ^3G_4$	$5f\,7p\ (5/2,3/2)_4$	86	88
59	$5f\,7p\ ^1G_4$	$5f\,7p\ (7/2,3/2)_4$	84	87
61	$5f\,7p\ ^3G_5$	$5f\,7p\ (7/2,3/2)_5$	93	100

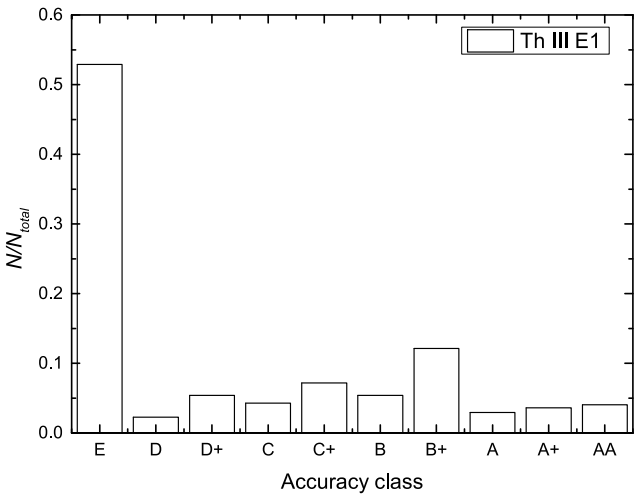

Figure 1. Distribution of E1 transitions over accuracy classes for Th III. The ratio of the number of transitions in a given accuracy class (N) to the total number ($N_{\rm total}$) of transitions in the y-axis is given.

to their experimental lifetimes. These transition probabilities are compared in Fig. 2. As we can see, despite a couple of transitions from state $5f7p\ ^3F_4$, the coincidence of probabilities is perfect. Our transition probabilities were also compared with probabilities from

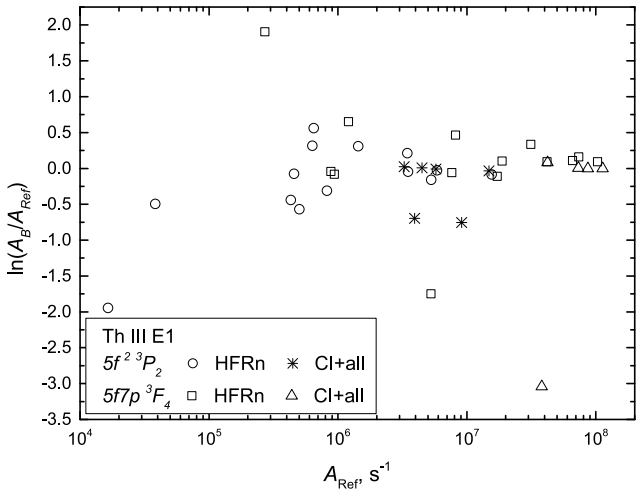

Figure 2. Comparison of our transition probabilities ($A_{\rm B}$) depopulating energy levels: $5f^2\ ^3P_2$ and $5f\,7p\ ^3F_4$ for which the radiative lifetimes have been measured by Biémont et al. (2002b) with probabilities normalized to these lifetimes ($A_{\rm HFRn}$) and with probabilities from CI+all method Safronova et al. (2014).

CI+all method Safronova et al. (2014) for the same states. Similarly to the comparison with Biémont et al. (2002b) results, only one transition disagrees.

A comparison of the lines strengths of Biémont et al. (2002b) that were computed with HFR (see Table 5 in reference to Biémont et al. 2002b) was also performed in Fig. 3. As can be seen, the agreement between the line strengths is satisfactory. Line strengths were also compared with data by Safronova et al. (2014) in Fig. 4. Two transitions disagree greatly with our computed one, while others agree well.

Line strengths are also compared with data from $S_{\rm SA-CASSCF}$ and $S_{\rm MS-CASPT2}$ methods computed by Roy et al. (2012) in Fig. 5. The line strengths are more scattered than the data from other methods.

Transition data are given in Table 7 (the complete table can be found in the Supporting Information). Level indexes (of lower and upper level No_l and No_u, respectively are the same as in the Tables 2 and 1), wavelengths, transition type, branching fractions $\left({\rm BF} = A_{ji}/\sum_{k=1}^{j-1} A_{jk}\right)$ (Wang et al. 2018), rates, weighted oscillator strengths, line strengths (the last three are given in the Babushkin and

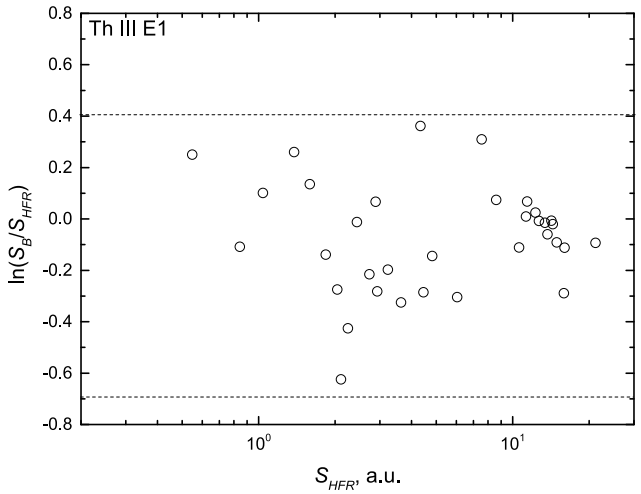

Figure 3. Comparison of our line strengths ($S_{\rm B}$) with computed using HFR method ($S_{\rm HFR}$) by Biémont et al. (2002b) for the strongest transitions.

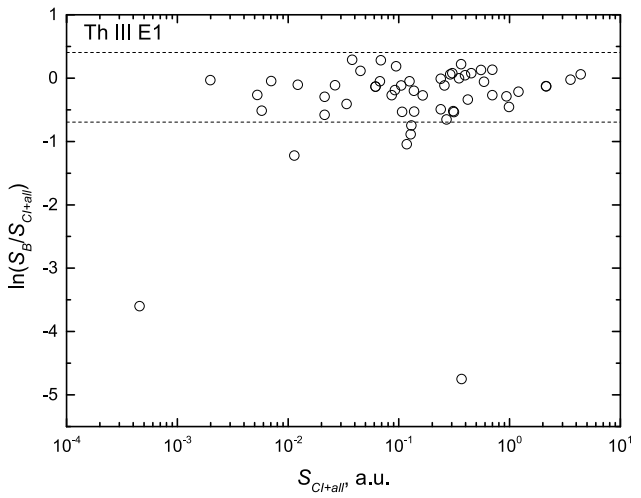

Figure 4. Comparison of our line strengths ($S_{\rm B}$) with computed using CI+all method ($S_{\rm CI+all}$) by Safronova et al. (2014).

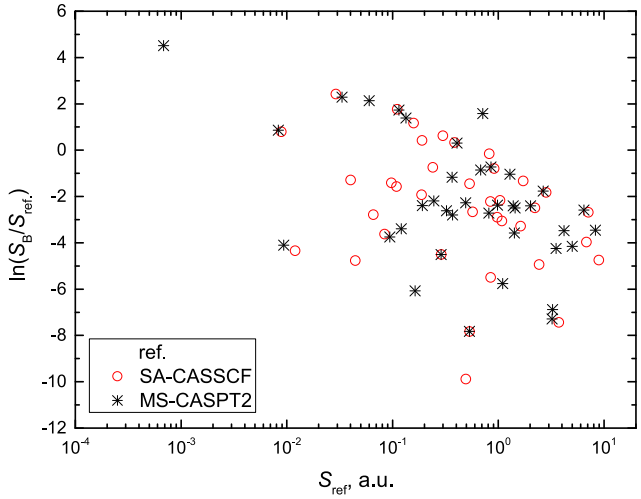

Figure 5. Comparison of our line strengths ($S_{\rm B}$) with $S_{\rm SA-CASSCF}$ and $S_{\rm MS-CASPT2}$ computed by Roy et al. (2012).

Table 6. Our computed lifetimes (in ns) in Babushkin and Coulomb gauges ($\mathrm{RCI}_{B,C}$) compared with CI+all calculations Safronova et al. (2014) and LIF experimental and HFR data by Biémont et al. (2002b).

Label	CI + all	HFR	LIF	RCI_B	RCI_C	RCI_{Bex}
$5f^2\ ^3P_2$	21.2	23.7	25.8 ± 1.5	26.48	39.70	27.52
$5f7p\ ^3F_4$	2.41	2.6	2.7 ± 0.2	2.35	2.27	2.46

Coulomb gauges) and accuracy classes for line strengths are provided in this table.

4.1 Lifetimes

Our computed lifetimes (τ) are compared with the measured values ($\tau_{\rm LIF}$) by Biémont et al. (2002b) in Table 6. In addition to our *ab-initio* RCI_B and RCI_C calculations, we have computed the lifetimes (RCI_{Bex}) using experimental wavelengths for transition probabilities. Lifetimes computed using HFR by Biémont et al. (2002b) are given in the same table. Safronova et al. (2014) have computed transition probabilities using experimental wavelengths and theoretical line strengths to evaluate the lifetimes ($\tau_{\rm CI+all}$). These lifetimes are compared with experimental ones in Table 6. The lifetime in the Babushkin gauge (RCI_B) of the first state is closer to the experimental value than the values of other methods. For the second state, the value in the Babushkin gauge is smaller than values from other methods.

5 APPLICATIONS TO KILONOVA SPECTRA

In this section, we apply our calculated transition data to kilonova spectra. To discuss the spectral features, we first calibrate the wavelengths of our transition data by cross-matching the transitions based on the LS terms. By this calibration, transition data used in this section have spectroscopically accurate wavelengths. When the wavelengths of the transitions are corrected, we also correct the line strength according to the energy difference ($S \propto \Delta E^{-3}$). However, this correction is insignificant and does not significantly impact the results as the accuracy in the energy is good enough.

Fig. 6 shows a comparison between the weighted oscillator strengths ($\log gf$) from the Babushkin gauge and those estimated by Domoto et al. (2024). The estimates by Domoto et al. (2024) are based on the emission line ratios measured in the thorium–argon hollow cathode lamp spectrum Engleman (2003) and calculated transition probabilities in optical wavelengths by Biémont et al. (2002a). As shown in the figure, our calculated gf values in the NIR wavelengths are generally smaller than those estimated by Domoto et al. (2024) by a factor of about 10.

We perform radiative transfer simulations using our transition data to study the impacts on the spectral features. We adopt the same setting of the calculations with Domoto et al. (2024). Namely, we assume a one-dimensional, spherical ejecta with a power-law density structure ($\rho \propto v^{-3}$). We adopt a spatially homogeneous abundance distribution. We use their 'Light' model for the abundance pattern, similar to metal-poor stars with weak r-process signature. In this abundance model, the mass fractions of the elements $Z > 50$ are reduced by a factor of about 100 concerning the solar abundance ratio). The mass fraction is 1.0×10^{-5}. For this model, we perform radiative transfer simulations using a time-dependent, wavelength-dependent radiative transfer code (Tanaka & Hotokezaka 2013; Kawaguchi, Shibata & Tanaka 2018). We use the same line list with Domoto et al. (2024) but adopt our transition data only for Th III lines. We refer the reader to Domoto et al. (2024) for more details.

Table 7. Transition wavelengths λ (in Å), branching fractions BF, transition rates A (in s^{-1}), weighted oscillator strengths gf, and line strengths S (in a.u.) in the Babushkin (B) and Coulomb gauges (C), accuracy classes (Acc. class) for E1 transitions of the Th III (The full table is available online as supplementary data).

No_l	No_u	λ (Å)	BF	A_B (s^{-1})	gf_B	S_B (a.u.)	A_C (s^{-1})	gf_C	S_C (a.u.)	Acc. class
1	7	24 025.06	2.004E−04	2.605E−01	1.578E−07	1.248E−05	6.533E + 02	3.957E−04	3.130E−02	E
1	16	15 084.46	4.439E−01	3.309E + 03	1.016E−03	5.045E−02	6.994E + 04	2.147E−02	1.066E + 00	E
1	25	9642.616	1.300E−01	7.661E + 03	7.475E−04	2.373E−02	8.834E + 03	8.620E−04	2.736E−02	C +
1	26	9579.755	3.207E−01	1.572E + 04	1.947E−03	6.139E−02	2.644E + 04	3.274E−03	1.032E−01	E
1	34	6832.501	4.274E−01	1.094E + 06	6.891E−02	1.550E + 00	3.438E + 05	2.166E−02	4.872E−01	E
1	37	5813.180	1.083E−04	2.585E + 02	1.441E−05	2.757E−04	5.341E + 03	2.977E−04	5.697E−03	E
1	41	4912.219	3.698E−04	3.052E + 03	7.728E−05	1.250E−03	1.063E + 01	2.691E−07	4.353E−06	E
1	42	4650.371	1.774E−01	1.695E + 06	4.946E−02	7.573E−01	7.584E + 05	2.213E−02	3.388E−01	E
1	45	3873.652	2.034E−01	2.731E + 06	5.529E−02	7.051E−01	1.278E + 06	2.588E−02	3.300E−01	E
1	51	2946.022	3.408E−01	1.425E + 08	1.298E + 00	1.259E + 01	1.429E + 08	1.301E + 00	1.262E + 01	AA

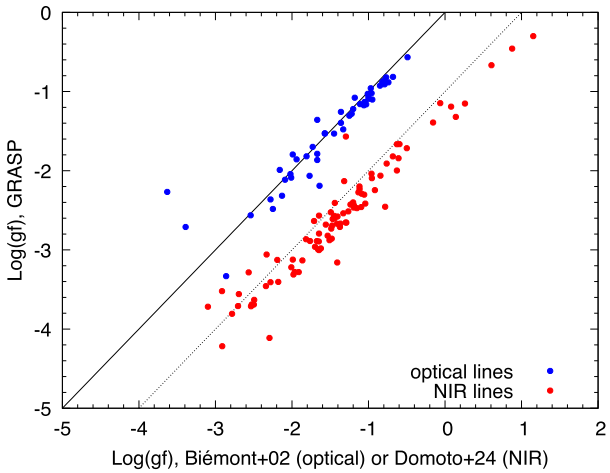

Figure 6. Comparison of our log gf values from the Babushkin gauge with those estimated by Domoto et al. (2024) for the lines listed in the NIST. Solid and dashed lines correspond to perfect agreement and deviation by a factor of 10, respectively.

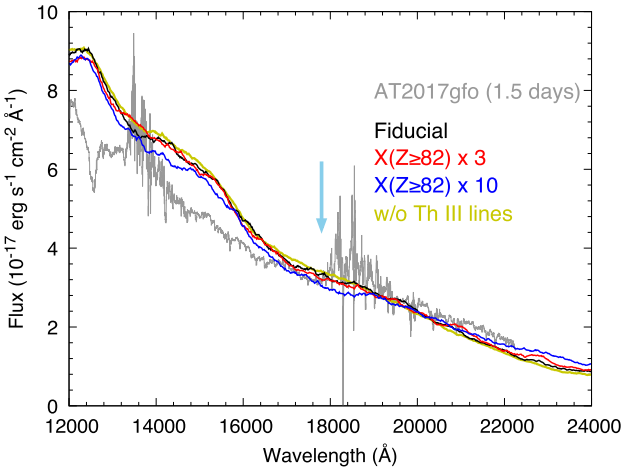

Figure 7. Synthetic spectra of a kilonova 1.5 d after the merger. The Black line shows the fiducial Light model results, while red and blue lines show the cases with enhanced mass fractions of the elements with $Z \geq 82$ by a factor of 3 and 10, respectively, and the dark-yellow line shows the case without the Th III lines. The light-blue arrow indicates the position of Th III absorption. The observed spectrum of AT2017gfo at 1.5 d after the merger (grey line, Pian et al. 2017; Smartt et al. 2017) is also compared.

Fig. 7 shows the synthetic spectra. The black line shows the spectra calculated with the fiducial Light model. Domoto et al. (2024) suggested that Th III lines can produce a broad absorption feature around 18 000 Å. However, our new calculations with our atomic data presented in this paper show that the appearance of the absorption features is marginal. This is because the gf values of the NIR transitions calculated in this paper tend to be lower than those adopted in Domoto et al. (2024) as shown in Fig. 6.

The red and blue lines in Fig. 7 show the synthetic spectra with the enhanced mass fraction of heaviest elements ($Z \geq 82$), including Th. If the mass fraction is enhanced by a factor of 3–10 as compared with our fiducial Light model (mass fraction of $(3 - 10) \times 10^{-5}$), kilonova spectra can show recognizable absorption features. Our calculations demonstrate the importance of accurate atomic data in connecting the observed depth of absorption features with the actual abundance in the ejecta.

6 SUMMARY AND CONCLUSIONS

A total of 63 energy levels were calculated and analyzed. In this study, the accuracy of the calculated energy levels was evaluated by comparing them with the experimental data. Our calculated energy levels matched the experimental data by RMS 436 cm^{-1} (two levels were excluded). Atomic states of the 5f7p configuration are more mixed than those of other configurations, and the identification is more complicated in $LS-$coupling. States of this configuration are much more pure in $JJ-$coupling.

In this work, 455 E1-type transitions between the energy levels of the configurations considered have been calculated. To evaluate the uncertainties of the calculated line strengths, the QQE method was employed, as described in references Gaigalas et al. (2022), Rynkun et al. (2022), and Kitovienė et al. (2024). According to the QQE method, 46 per cent fall into the D and better accuracy class. Our computed line strengths agree well with data computed by Safronova et al. (2014), and even better with results by Biémont et al. (2002b).

Finally, we showed that kilonova spectra can show recognizable absorption features of Th III lines with a Th abundance of $(3 - 10) \times 10^{-5}$. Our work demonstrates the importance of accurate atomic data in determining the mass fraction of heavy elements from observed absorption features.

ACKNOWLEDGEMENTS

This project has received funding from the Research Council of Lithuania (LMTLT), agreement no. S-LJB-23-1 and JSPS Bilateral Joint Research Project (JPJSBP120234201).

DATA AVAILABILITY

The data (Table 7) underlying this article are available in the article and its online Supporting Information.

REFERENCES

Abbott B. P. et al., 2017, ApJ, 848, L12
Berengut J. C., Dzuba V. A., Flambaum V. V., Porsev S. G., 2009, Phys. Rev. Lett., 102, 210801
Biémont E., Quinet P., Ryabchikova T. A., 2002a, MNRAS, 336, 1155
Biémont E., Palmeri P., Quinet P., Zhang Z. G., Svanberg S., 2002b, ApJ, 567, 1276
Blaise J., Wyart J.-F., 1992, Energy Levels and Atomic Spectra of Actinides, International Tables of Selected Constants, Vol. 20. Centre National de la Recherche Scientifique, Paris, France 1
de Bruin T. L., Klinkenberg P. F. A., 1940, Proc. Roy. Acad. Amsterdam, 43, 581
de Bruin T. L., Klinkenberg P. F. A., Schuurmans P., 1941, Z. Phys., 118, 58
Chornock R. et al., 2017, ApJ, 848, L19
Cowan R. D., 1981, The Theory of Atomic Structure and Spectra. University of California Press, Berkeley, CA, USA
Cowan J. J., Sneden C., Lawler J. E., Aprahamian A., Wiescher M., Langanke K., Martínez-Pinedo G., Thielemann F.-K., 2021, Rev. Mod. Phys., 93, 015002
Domoto N., Tanaka M., Wanajo S., Kawaguchi K., 2021, ApJ, 913, 26
Domoto N., Tanaka M., Kato D., Kawaguchi K., Hotokezaka K., Wanajo S., 2022, ApJ, 939, 8
Domoto N. et al., 2023, ApJ, 956, 113
Domoto N., Wanajo S., Tanaka M., Kato D., Hotokezaka K., 2024, ApJ, 978, 99
Engleman R., Jr, 2003, J. Quant. Spec. Radiat. Transf., 78, 1
Fischer C. F., Godefroid M., Brage T., Jönsson P., Gaigalas G., 2016, J. Phys. B: Atom. Mol. Opt. Phys., 49, 182004
Fontes C. J., Fryer C. L., Hungerford A. L., Wollaeger R. T., Korobkin O., 2020, MNRAS, 493, 4143
Fontes C. J., Fryer C. L., Wollaeger R. T., Mumpower M. R., Sprouse T. M., 2023, MNRAS, 519, 2862
Gaigalas G., 2020, Comput. Phys. Commun., 247, 106960, available at: https://doi.org/10.1016/j.cpc.2019.106960
Gaigalas G., Rudzikas Z., Fischer C. F., 1997, J. Phys. B: Atom. Mol. Opt. Phys., 30, 3747
Gaigalas G., Fritzsche S., Grant I. P., 2001, Comput. Phys. Commun., 139, 263, available at: https://doi.org/10.1016/S0010-4655(01)00213-2
Gaigalas G., Fischer C. F., Rynkun P., Jönsson P., 2017, Atoms, 5, 6
Gaigalas G., Rynkun P., Banerjee S., Tanaka M., Kato D., Radžiūtė L., 2022, MNRAS, 517, 281
Gaigalas G., Rynkun P., Domoto N., Tanaka M., Kato D., Kitovienė L., 2024, MNRAS, 530, 5220
Gillanders J. H., Smartt S. J., Sim S. A., Bauswein A., Goriely S., 2022, MNRAS, 515, 631
Gillanders J. H., Sim S. A., Smartt S. J., Goriely S., Bauswein A., 2024, MNRAS, 529, 2918
Grant I. P., 2007, Relativistic Quantum Theory of Atoms and Molecules. Springer-Verlag, Berlin
Holmbeck E. M., Sprouse T. M., Mumpower M. R., Vassh N., Surman R., Beers T. C., Kawano T., 2019, ApJ, 870, 23
Hotokezaka K., Tanaka M., Kato D., Gaigalas G., 2023, MNRAS, 526, L155
Jönsson P. et al., 2023, Atoms, 11, 68
Kawaguchi K., Shibata M., Tanaka M., 2018, ApJ, 865, L21
Kitovienė L., Gaigalas G., Rynkun P., Tanaka M., Kato D., 2024, J. Phys. Chem. Reference Data, 53, 033101
Kramida A., Ralchenko Yu., Reader J., NIST ASD Team, 2021, NIST Atomic Spectra Database (ver. 5.9), [Online]. National Institute of Standards and Technology, Gaithersburg, MD, https://physics.nist.gov/asd
Martin W., Wiese W., 1996, Atomic, Molecular, and Optical Physics Hand-Book. AIP Press, Woodbury, NY, available at: http://www.nist.gov/pml/pubs/atspec/index.cfm
Pian E. et al., 2017, Nature, 551, 67
Pognan Q., Wu M.-R., Martínez-Pinedo G., Ferreira da Silva R., Jerkstrand A., Grumer J., Flörs A., 2024, MNRAS, 536, 2973
Radžiūtė L., Gaigalas G., 2023, Atomic Data and Nuclear Data Tables, 152, 101585, available at: https://doi.org/10.1016/j.adt.2023.101585
Radžiūtė L., Gaigalas G., Kato D., Rynkun P., Tanaka M., 2020, ApJS, 248, 17
Radžiūtė L., Gaigalas G., Kato D., Rynkun P., Tanaka M., 2021, ApJS, 257, 29
Redman S. L., Nave G., Sansonetti C. J., 2014, ApJS, 211, 4
Roy S., Prasad R., Datta S. N., Chandra P., 2012, Chem. Phys. Lett., 550, 25, available at: https://doi.org/10.1016/j.cplett.2012.08.048
Rynkun P., Banerjee S., Gaigalas G., Tanaka M., Radžiūtė L., Kato D., 2022, A&A, 658, A82, available at: https://doi.org/10.1051/0004-6361/202141513
Safronova M. S., Safronova U. I., Clark C. W., 2014, Phys. Rev. A, 90, 032512
Smartt S. J. et al., 2017, Nature, 551, 75
Sneppen A., Watson D., 2023, A&A, 675, A194
Tanaka M., Hotokezaka K., 2013, ApJ, 775, 113
Tanaka M. et al., 2023, ApJ, 953, 17
Wanajo S., Fujibayashi S., Hayashi K., Kiuchi K., Sekiguchi Y., Shibata M., 2024, Phys. Rev. Lett. , 133, 241201
Wang K., Jönsson P., Gaigalas G., Radžiūtė L., Rynkun P., Del Zanna G., Chen C. Y., 2018, ApJS, 235, 27
Watson D. et al., 2019, Nature, 574, 497
Wyart J. F., Kaufman V., 1981, Phys. Scr., 24, 941

SUPPORTING INFORMATION

Supplementary data are available at *MNRAS* online.

Table 7. Transition wavelengths λ (in Å), branching fractions BF, transition rates A (in s^{-1}), weighted oscillator strengths gf, and line strengths S (in a.u.) in the Babushkin (B) and Coulomb gauges (C), accuracy classes (Acc. class) for E1 transitions of the Th III.

Please note: Oxford University Press is not responsible for the content or functionality of any supporting materials supplied by the authors. Any queries (other than missing material) should be directed to the corresponding author for the article.

This paper has been typeset from a TEX/LATEX file prepared by the author.